

AD-A251 425



2

**MICROSTRUCTURAL DEVELOPMENT IN A  
SPRAY FORMED ALUMINUM-SILICON  
CARBIDE BASED METAL MATRIX COMPOSITE**

**First Annual Progress Report**

**Grant No. N00014-91-J-1648**  
MAY 1992

**S DTIC ELECTE D**  
JUN 10 1992  
**A**

This document has been approved  
for public release and sale; its  
distribution is unlimited.

**Submitted by**  
**Paul R. Howell**

**Professor of Metals Science**  
**The Pennsylvania State University**  
**University Park, PA16802**

92 5 14 038

**92-12920**  


Forward

A graduate student(Xiaoli Tang) started on this project on September 1, 1991. Included in this report are the preliminary findings concerning the investigation on the nature of spray formed aluminum-silicon carbide based metal matrix composite. In light of the fact that grain boundary precipitation (both low-angle and high-angle) is of the utmost importance, we have examined the interaction between grain boundaries and the precipitation of plate-like phases in both Al-based, and other alloys. The results of the investigation are included as a preprint for publication in the conference proceeding "ALUMINUM ALLOYS: Their Physical and Mechanical Properties". Finally, an abstract of a paper which will be presented at the American Society for Composite, Seventh Technical Conference on Composite Materials, is included.



Accession For	
NTIS	<input checked="" type="checkbox"/>
CRA&I	<input type="checkbox"/>
DTIC	<input type="checkbox"/>
TAB	<input type="checkbox"/>
Unannounced	<input type="checkbox"/>
Justification .....	
By .....	
Distribution /	
Availability Codes	
Dist	Avail and/or Special
A-1	

Statement A per telecon  
Dr. Asuri Vasudevan ONR/Code 1222  
Arlington, VA 22217-5000  
NWW 6/9/92

The materials used in this research were provided by the Office of Navy research. Upon receiving these samples at the beginning of last October, the following work has been performed.

1. Aging curves of 8090 control alloy and 8090-SiC composites at 190°C

The ultimate goal of this study is to correlate the microstructures with mechanical properties. Hence, it is necessary to know the aging response of both the control alloy and the composite. The aging kinetics curves are shown in Fig.1.

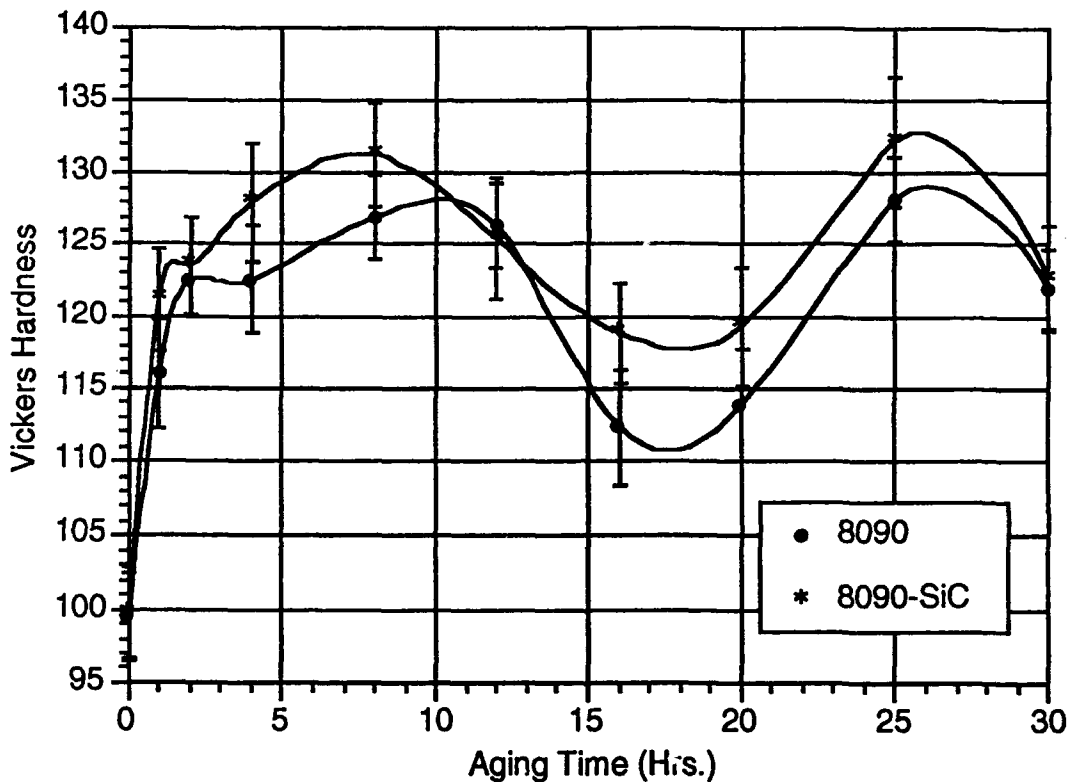


Fig.1 Aging Kinetic Curves

In comparing the aging kinetics of 8090 control alloy, the addition of SiC doesn't change the aging kinetics and the microhardness appreciably. Meanwhile, both materials exhibit a double maxima. It can be expected that the first maximum is due to the hardening effect of  $\delta'(Al_3Li)$ , the second maximum from the effect of  $S'(Al_2CuMg)$ .

2. SEM observations on the size and distribution of SiC

SEM images of the composite are shown in Fig.2. From the micrograph, it can be seen that:

- a) the distribution of the SiC particles is not uniform. Some regions are almost free of SiC particle, and the other regions contain clusters of SiC.
- b) The size of the SiC varies. Most of the SiC particles have diameters of about 3-4 $\mu\text{m}$ , and the rest are very coarse particles sized around 10 $\mu\text{m}$ . The shape of the particles is irregular.

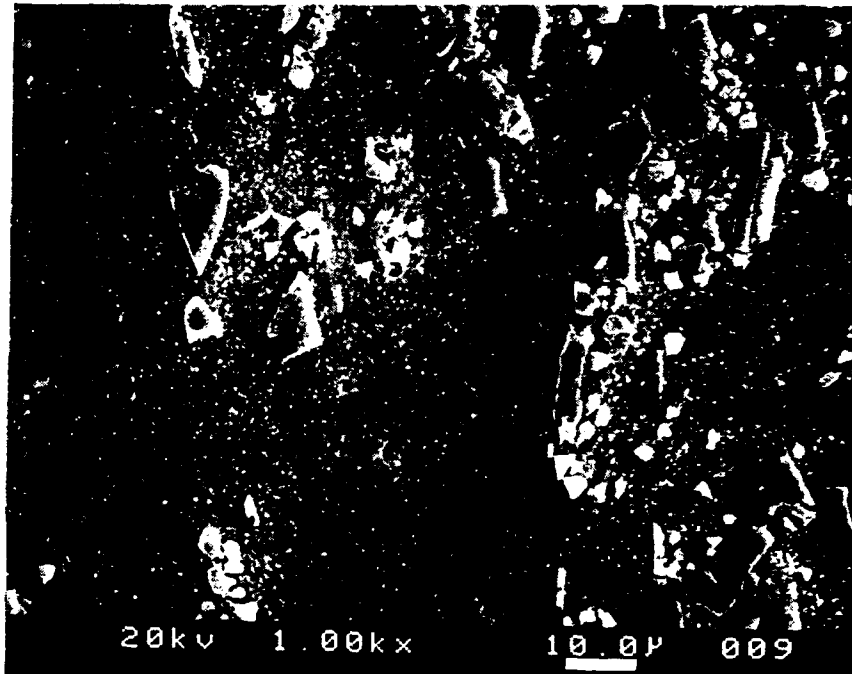


Fig. 2 Distribution of the SiC particles

Fig. 3 shows elongated grains, and the grain boundaries are seen to be decorated with some precipitates. In addition, some of the rod-like SiC particles are oriented parallel to the long axis of the grains. The latter is predominantly parallel to the extrusion direction.

### 3. TEM observation of precipitates in the control alloy 8090 and the 8090+SiC composite

The TEM sample of the control alloy was prepared with a conventional electro-polishing method. The sample was twin-jetted in a solution of 30% nitric acid plus 70% methanol at about -30°C. This method was very effect for preparing the

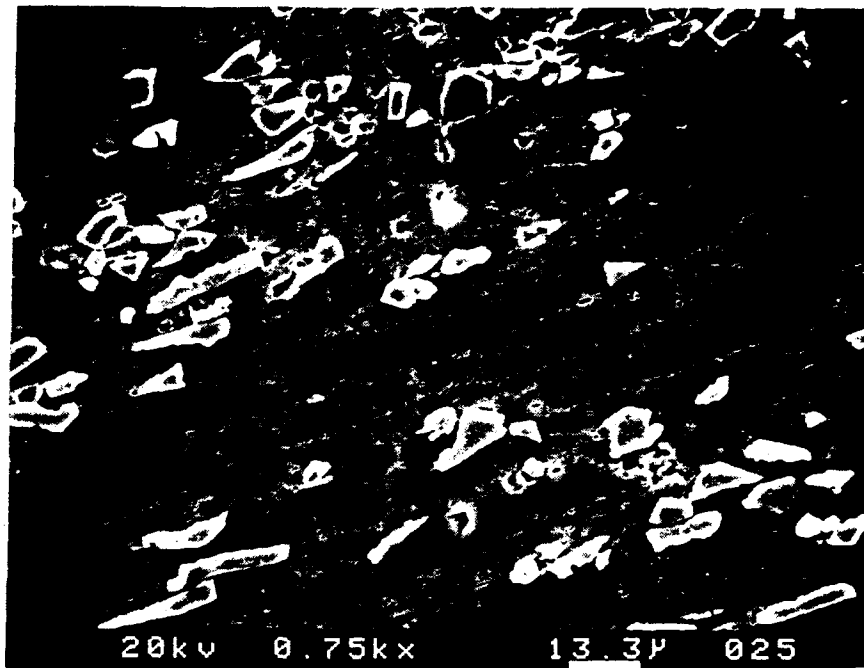


Fig. 3 Elongated grains and oriented precipitates

TEM sample of the 8090 control alloy. The same procedure failed to give a satisfactory sample of the 8090-SiC composite. The matrix was thinned but the SiC particles were not. Hence, the interface of matrix/SiC could not be seen clearly. To make a suitable sample of the composite, the ion milling was used. To avoid the possible heating effect, in the ion milling procedure, on the aging behavior of the composite, a cold stage, cooled by liquid nitrogen, was used when the sample was prepared.

In order to observe the microstructural changes at the matrix/SiC interface, the samples aged 20 hours at 190°C were first examined with TEM. According to our preliminary observations, no obvious precipitates existed at the interface after aged 20 hours at 190°C. For both the control alloy and composite,  $\delta'$  was the most frequently observed precipitate in the matrix. Fig.4 is a DF image of  $\delta'$  in the control alloy. It can be seen that after 20 hrs. aging at 190°C, the density of  $\delta'$  is very high. While a  $\delta'$  PFZ (precipitate free zone) is obvious along the high angle boundary. This means some other precipitates (most probably  $T_2$ ) formed at the boundary, which consumed the  $\delta'$  next to the high angle boundary.

Fig. 5 is the another DF image of the same sample. From this micrograph, the duplex  $\delta'/\beta'$  precipitate can be seen very clearly. The dark centers in the duplex precipitate is  $\beta'$ , and the  $\delta'$  encapsulates the  $\beta'$ . This is because the  $\beta'$  forms during solidification process. Since the crystal structures and the parameters of  $\beta'$  are very close to those of  $\delta'$ , the interface of  $\beta'$ /matrix is an effective site for the

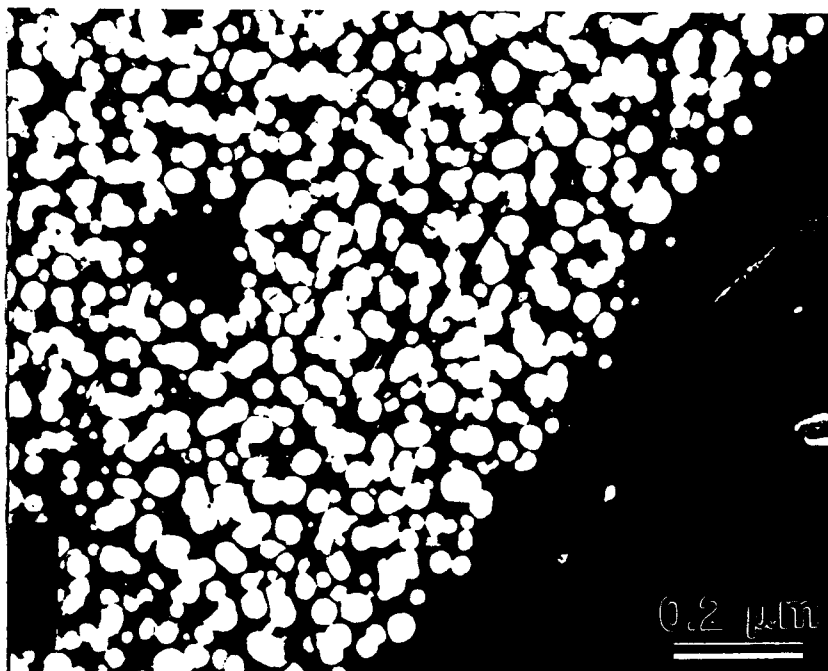


Fig. 4  $\delta'$  in the control alloy aged at 190°C for 20 hrs. A  $\delta'$  PFZ along the high angle boundary is very obvious.

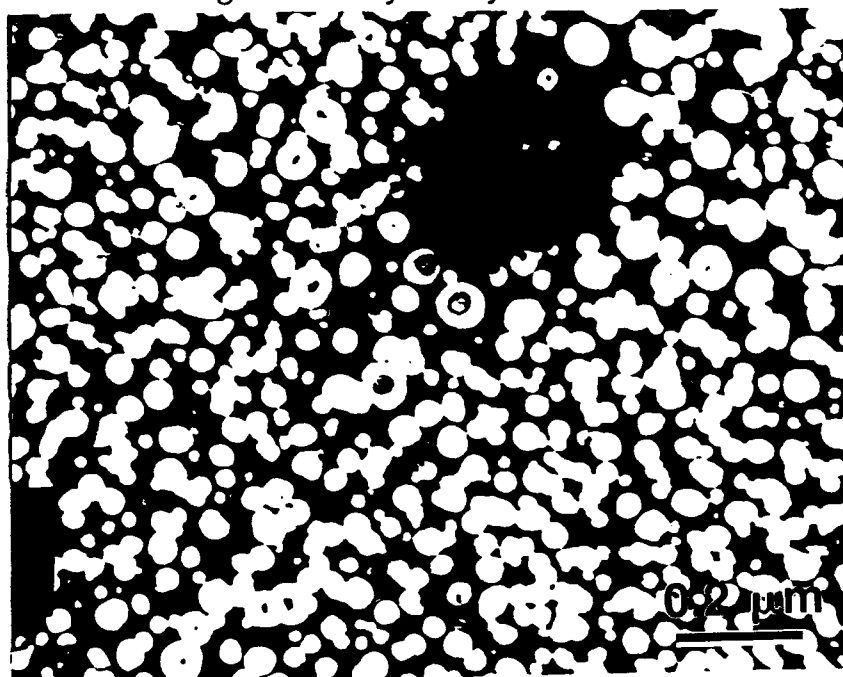


Fig. 5  $\delta'/\beta'$  complex precipitates in the control alloy aged at 190°C for 20 hrs.  $\delta'$  free region near the top of the picture is due to the existence of T2.

nucleation and growth of  $\delta'$ . Towards the top of this picture, there is a  $\delta'$  free region, which is caused by a T2 precipitate. In the BF image from the same region(see Fig.6), the T2 precipitate can be seen clearly. Note that the T2 particle has transformed to a microcrystalline aggregate.

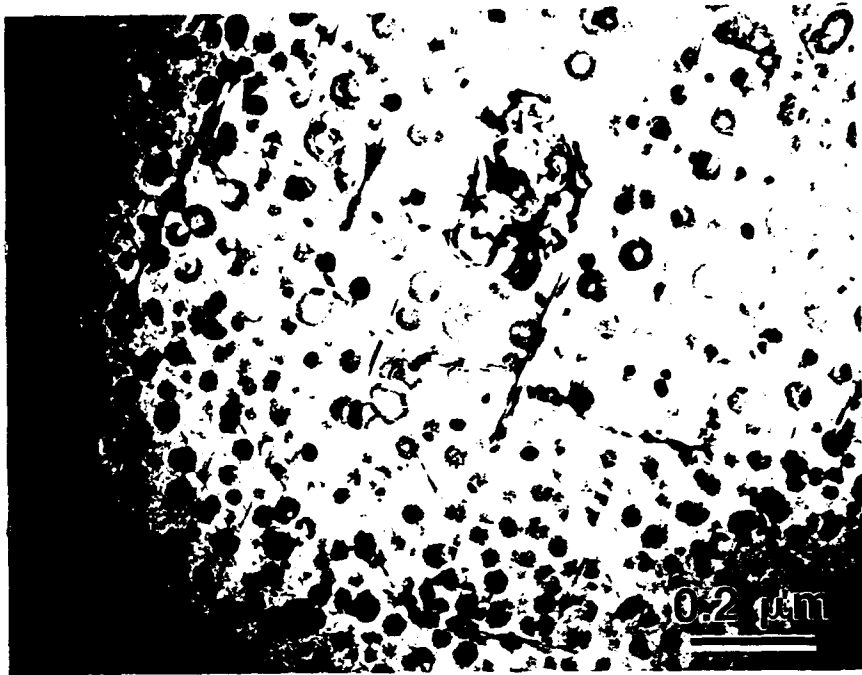


Fig. 6 BF image of T<sub>2</sub>. (from the same region shown in Fig. 5)

Fig 7 is another BF image of the control alloy which shows that plate-like precipitates have formed after 20 hours aging. The streaks accompanying the diffraction pattern indicate that the precipitates are S'. Fig. 8 is a diffraction pattern of the control alloy. The streaks in  $\langle 201 \rangle$  direction are from the S' phase. The streaks from  $\theta'$  and T<sub>1</sub> can be seen in some other diffraction patterns.

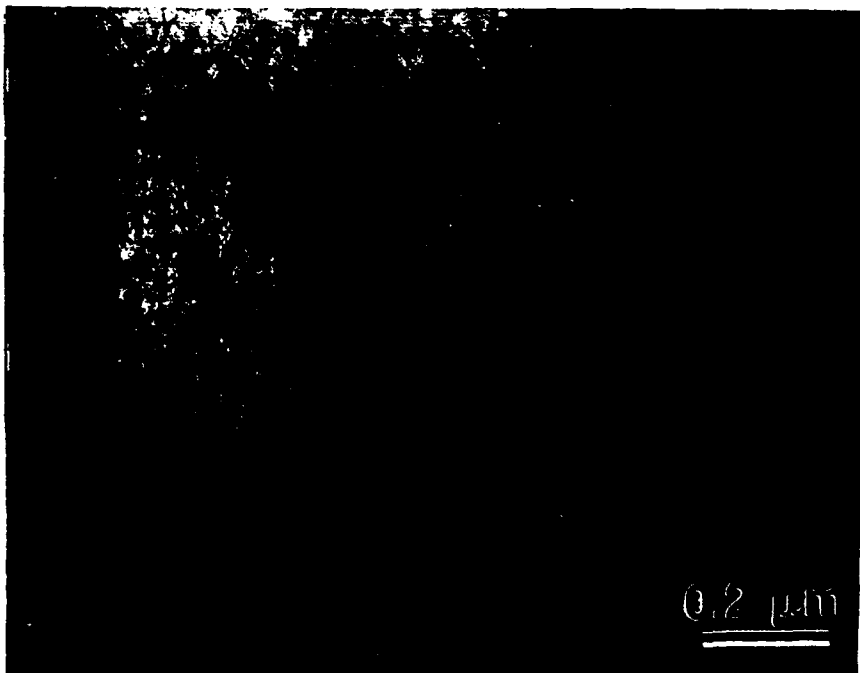


Fig. 7 BF image of plate-like precipitates in the control alloy aged at 190°C for 20 hrs.

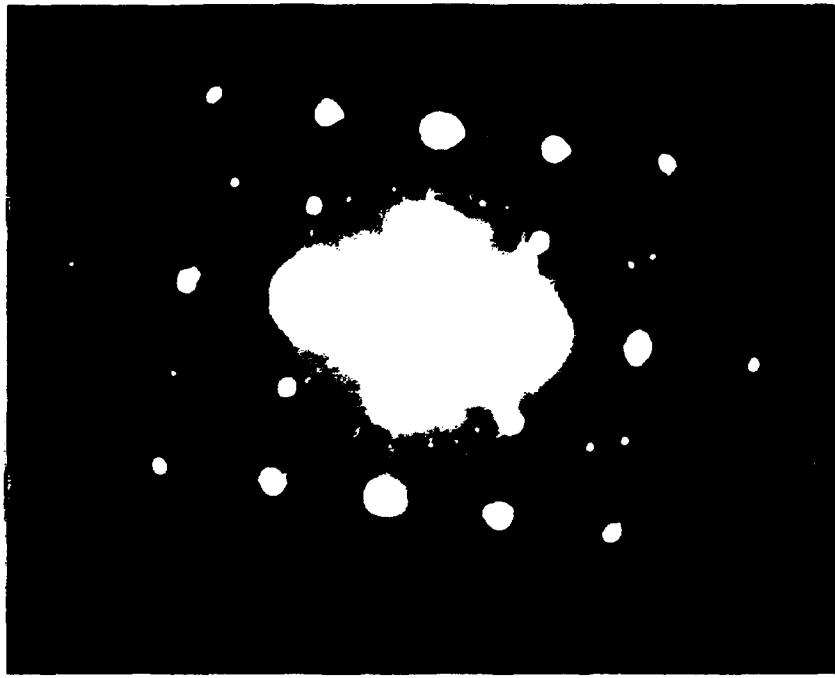


Fig. 8 A diffraction pattern from the control alloy aged at 190°C for 20 hrs. The main spots are from matrix and  $\delta'$ , and the streaks in  $\langle 201 \rangle$  direction are from  $S'$ .

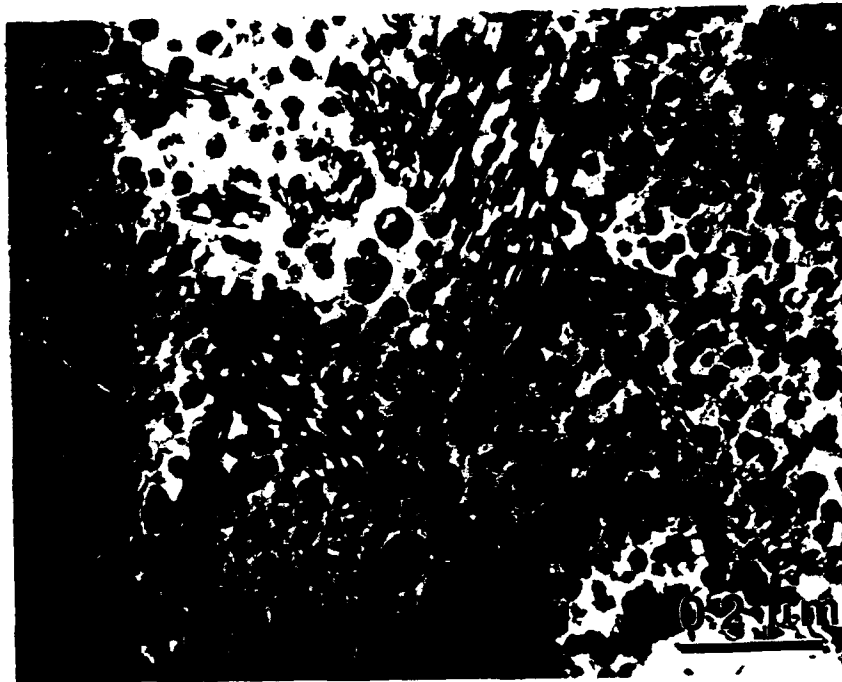


Fig. 9 BF imaged from the same region as Fig. 8  
(control alloy aged 20 hrs. at 190°C)

Fig. 9 is a BF image from the region which yields the diffraction pattern of Fig. 8. The spherical precipitates are  $\delta'$  and the plate-like phases are  $S'$ .

Fig. 10 is a DF image of  $\theta'$  from the control alloy. Note the low volume fraction of the phase.



Fig. 10 DF image of  $\theta'$  from the control alloy aged at 190°C for 20 hrs.

The composite has been also examined with TEM. The  $\delta'$  distribution is shown in Fig. 11. Compared to the control alloy, the density of  $\delta'$  in the composite is lower.

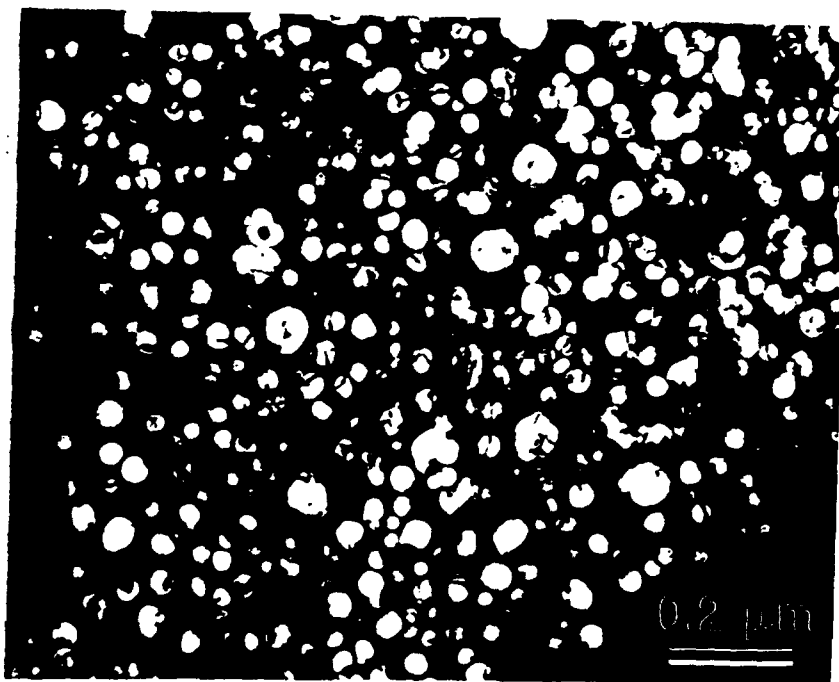


Fig. 11 DF image of  $\delta'$  in the composite aged at 190°C for 20 hrs.

Due to the high dislocation density in the matrix of composite, the contrast in BF mode is very complex, no precipitates can be identified clearly in the BF image(see Fig. 12).

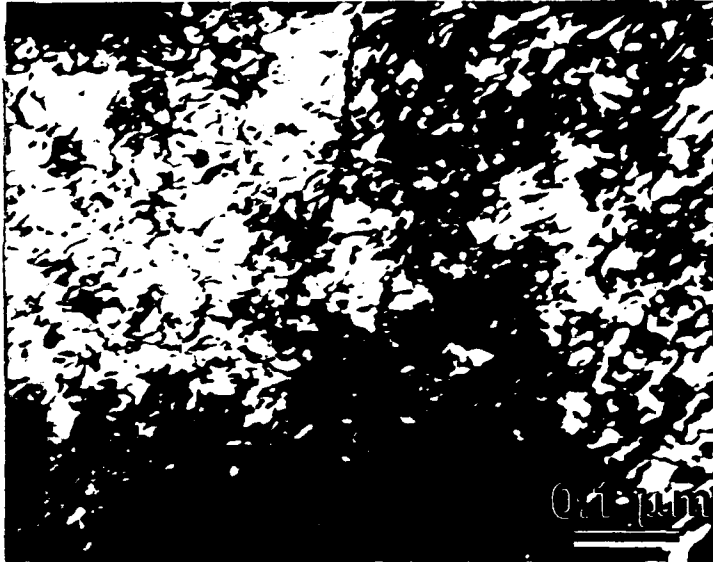


Fig. 12 BF image from the matrix of the composite, aged at 190°C for 20 hrs.

### Proposed Research Program

Over the next twelve months, the microstructure of the composite and control alloys will be fully characterized both qualitatively and quantitatively.

We will also seek to answer the following question: Why are the aging kinetics, and peak hardness of the two materials, virtually identical. One plausible hypothesis concerns offsetting influences of the SiC particles. On the one hand, precipitation at the SiC interface may tend to render the composite less age hardenable. Conversely, the higher dislocation density in the composite could well facilitate the formation of e.g.,  $\theta'$ , T1 and S'. Hence, one of our major aims is the quantitative analysis of the precipitation of these plate-like phases.

## THE PRECIPITATION OF PLATE LIKE PHASES IN Al-BASED AND OTHER ALLOYS

X. Tang\* M. H. Tosten\*\* and P. R. Howell\*

\*Department of Materials Science and Engineering, The Pennsylvania State University,  
University Park, PA 16802

\*\*Westinghouse Savannah River Laboratories, Aiken, SC 29808 USA

### INTRODUCTION AND BACKGROUND

The nucleation of plate-like phases at grain boundaries had been known to occur for a long time. For example, Vaughan [1] investigated an Al-Cu alloy in detail, and found that  $\theta'$  formed, predominantly at low angle boundaries and that the number density of precipitates decreased as the angle of misorientation increased. In addition, Vaughan documented a single orientation of  $\theta'$  on a given segment of boundary and reported that this single variant minimized the angle between the habit plane ( $\{001\}_\alpha \parallel \{001\}_{\theta'}$ ) and the local boundary plane. It was suggested that this orientation formed since it produced the largest reduction in strain energy; a claim that was substantiated by subsequent elastic energy calculations [2]. Aaronson et al., [3] summarized the available data up to (1971) and concluded that for misorientations less than  $10^\circ$  only primary sideplates (Widmanstätten plates) formed. Table 1 (modified from reference [3]) lists the systems for which plate like phases had been found to nucleate on low-angle grain boundaries.

Alloy	Precipitate	Angular Range
Al-4% Cu	$\theta'$ (complex bct)	0-12°
Fe -0.29%C	$\alpha$ (bcc)	-
Al-18% Ag	$\gamma'$ (hcp)	0-17°
Ag-5.6% Al	$\beta$ (bcc)	0-14°
Al-6.7% Zn -2.5-3% Mg	$\eta'$ (hcp)	-
Co-20% Fe	$\alpha$ (bcc)	-

In 1975, Lee and Aaronson [4,5] presented a careful mathematical analysis on the effect of faceting on grain boundary precipitation, and showed that as the angle between the habit plane and the grain boundary plane, ( $\theta$ ), decreased, then so did the energy barrier to nucleation ( $\Delta G^*$ ). Figure 1 is a modified version of one of Lee and Aaronson's plots of  $\Delta G^*/\Delta G^*_s$  as a function of  $\theta$  (where  $\Delta G^*_s$  is the energy barrier for nucleation for an unfaceted allotriomorph). Note that  $\Delta G^*$  shows a rapid increase with  $\theta$ , particularly when the relative interfacial energy of the facet (habit plane) is small.

In Lee and Aaronson's papers, the simplifying assumption of ignoring strain energy was invoked, and minimization of interfacial free energy was the major criterion. In (1986), Park and Ardell [6] interpreted their results, on the grain boundary precipitation of the  $\eta$  phase in a commercial Al alloy (7075), in terms of the analyses presented in refs. [4,5]. However, it was also noted in [6] that, for low angle grain boundaries, the  $\eta$  precipitates adopted "well defined plate shaped morphologies."

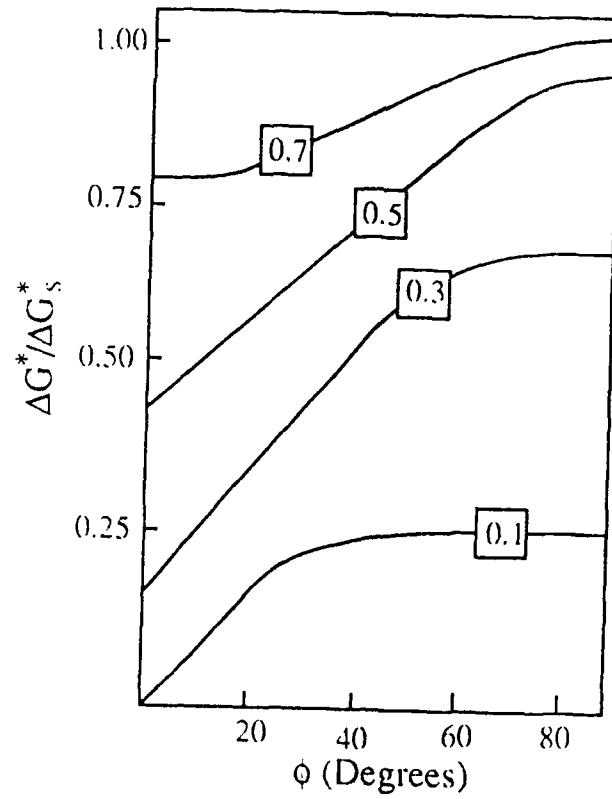


FIG 1. The energy barrier to nucleation for a faceted grain boundary nucleus as a function of  $\phi$  (Adapted from Lee and Aaronson [5]. The four curves are for different values of  $\gamma_c/\gamma_{\alpha\beta}$  where  $\gamma_{\alpha\beta}$  is the facet energy.

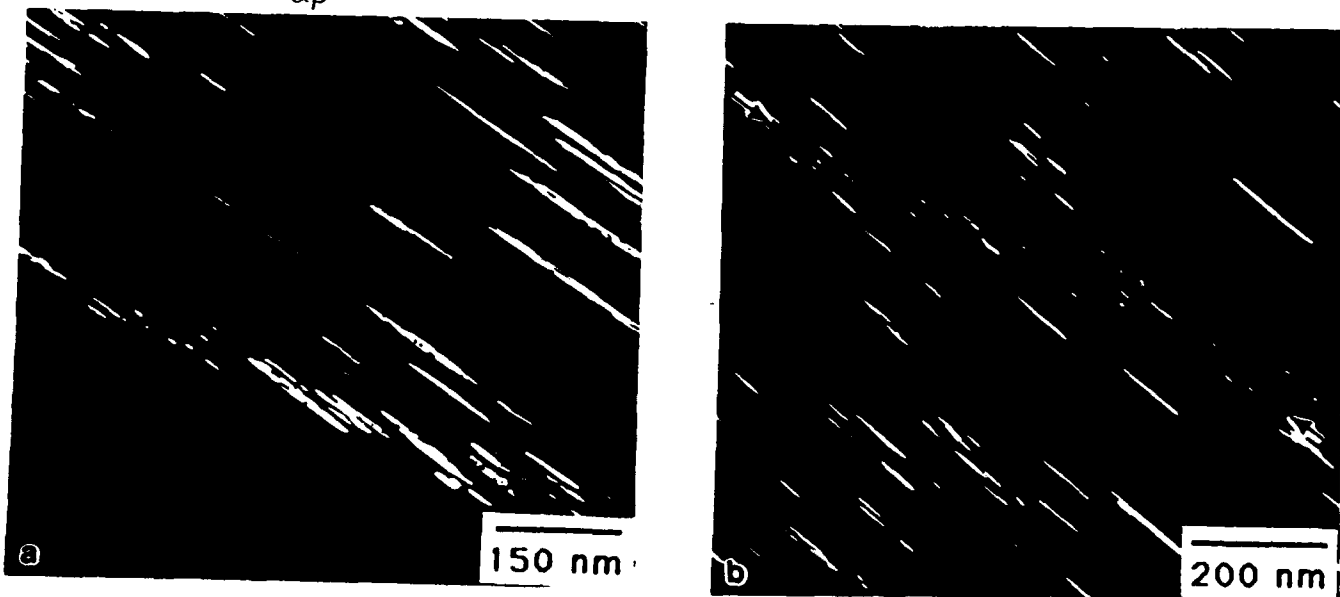


FIG 2. Precipitation of  $T_1$  and  $\theta'$  on sub-boundaries. a)  $T_1$  centered dark field (CDF) image b)  $\theta'$  CDF image.

More recently, Luo and Weatherly [7] and Monzen and Kitagawa [8] analyzed the nucleation behavior of b.c.c. precipitates on grain boundaries in an fcc matrix. In both instances, faceting of the precipitates was observed and the habit planes were quoted as:

$$\{121\}_f \parallel \{312\}_b \text{ ref. [7]}$$

$$\{111\}_f \parallel \{110\}_b \text{ ref. [8]}$$

Where the subscripts f and b refer to fcc and bcc respectively. Both studies presented results which were fully consistent with the theoretical predictions of Lee and Aaronson [4.5] in that for general high angle grain boundaries:

- (i) the variant(s) adopted on any given boundary was that which was characterized by the smallest angle between the habit plane and local boundary plane and,
- (ii) as the angle between the low energy facet and the boundary plane increased, the number density of the precipitates decreased.

From the above, it would appear that there are two conflicting viewpoints concerning the efficacy of low and high angle grain boundaries as nucleation sites for plate-like precipitates. The results of e.g., Vaughan [1] show that as the angle of misorientation increases, then the nucleation frequency decreases, whereas the result of e.g., Monzen and Kitagawa [8] show the reverse trend.

In the present paper, grain boundary precipitation of  $T_1$  ( $Al_2CuLi$ ) and  $\theta'$  ( $Al_2Cu$ ), in an Al- 3% Cu- 2% Li- 0.12% Zr alloy, is analyzed. The data will be used to present a rationale for the effect of grain boundary misorientation on the nucleation of plate like precipitates.

## EXPERIMENTAL

The experimental alloy, whose composition is given in Table 2, was provided by the Alloy Technology Division of Alcoa Laboratories, Alcoa Center, PA.

Table 2. Composition of the Experimental Alloy						
Li	Cu	Zr	Fe	Si	Ti	Al
2.1	2.9	0.12	0.06	0.06	0.01	balance

The alloy was solution treated at 550°C for 30 minutes and subsequently aged at 190°C for 120 hours.

Specimens for transmission electron microscopy (TEM) were prepared in a twin-jet electropolisher using a 25% nitric acid -75% methanol solution at -20°C and at an applied potential of about 12V. After perforation, the thin foils were washed in a steady stream of ethanol for one minute and subsequently examined using a Philips EM420T at 120kV.

Grain boundary misorientations were determined using a low camera length, convergent beam electron diffraction (LCL-CBED) technique [9] which employed Kikuchi lines, centers and higher order Laue zones. This technique yields an accuracy of better than 0.5°.

## RESULTS

In general, sub-boundaries (arbitrarily defined as  $\theta < 1$ ) were excellent nucleation sites for both  $T_1$  and  $\theta'$ . Figures 2 a,b are  $T_1$  and  $\theta'$  centered dark fields (CDFs) respectively and show that there is a high number density of these plate like phases. Reference to figure 2a also shows that the precipitates on the sub-boundaries often tended to be shorter, but thicker than the intragranular precipitates. As the misorientation increased, there was a rapid decline in the number density of

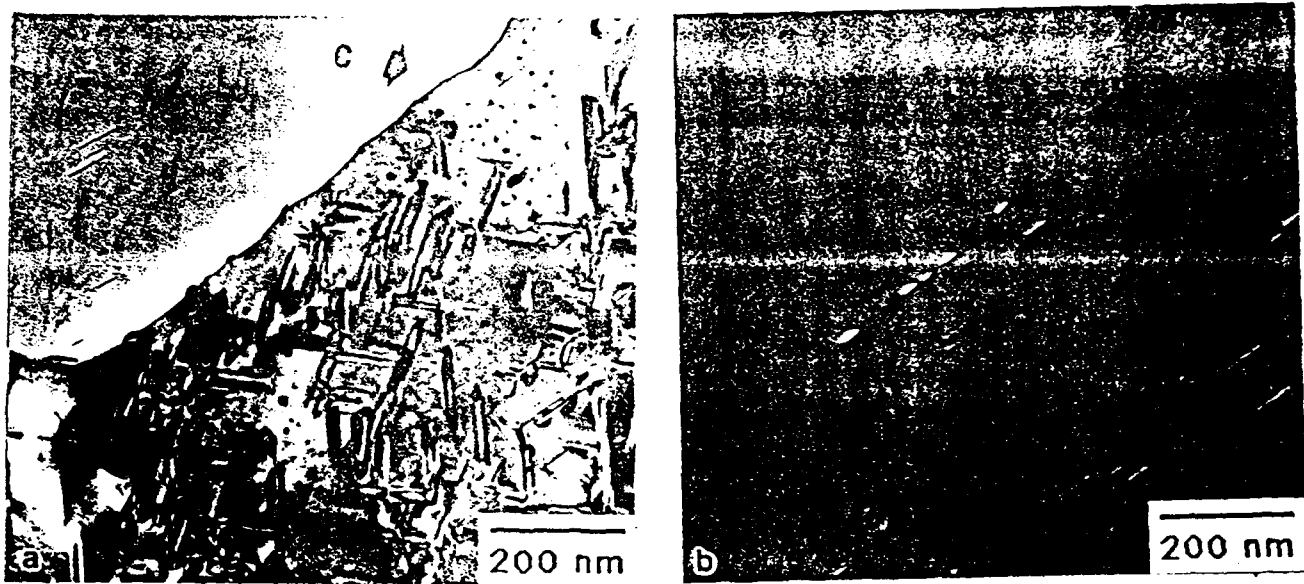


FIG 3. Bright field (BF)/ $\theta'$  CDF images of precipitation on a low angle grain boundary. a) BF image. Note the  $\delta'$  precipitate free zone at C. b)  $\theta'$  CDF image. Note that the  $\theta'$  habit plane is at a low angle to the grain boundary plane.

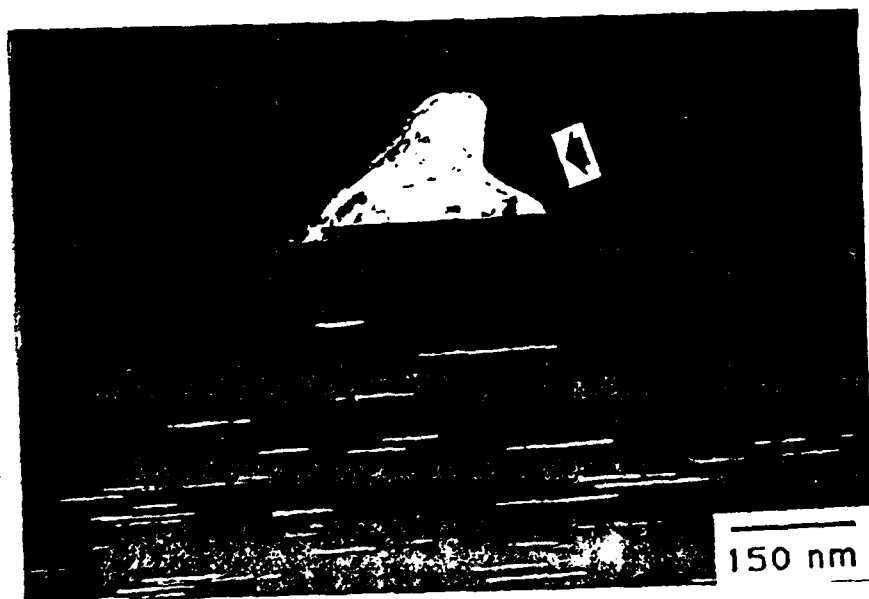


FIG 4. A  $T_1$  precipitate on a triple junction.

both the  $T_1$  and  $\theta'$ . Figures 3a,b are a bright field/ $\theta'$  dark field pair of a low-angle grain boundary for which the misorientation is  $6.5^\circ$ . A  $\delta'$  precipitate free zone is evident at C. The intergranular  $\theta'$  are related to the lower, right-hand grain but have grown predominantly into the upper, left-hand grain. This should be contrasted with precipitation on sub-boundaries where growth appeared to occur equally into both grains. Reference to figures 2-3 also shows that the angle between the habit plane and the local boundary plane is low.

$T_1$  was rarely observed on high angle grain boundaries; one of those occurrences is presented in the  $T_1$  centered dark field image of figure 4. The single  $T_1$  precipitate is located at a triple junction, is related to the lower grain, and has grown smoothly into the other two grains. Finally, figure 5 shows another high angle grain boundary and several  $T_2$  ( $Al_6CuLi_3$ ) precipitates are arrowed.

## DISCUSSION AND SUMMARY

The results of the present investigation are completely in agreement with the earlier investigation of Vaughan and can be explained in exactly the same fashion i.e., nucleation occurs on low angle grain boundaries as opposed to homogeneously, due to the reduction in strain energy, not interfacial energy. Hence, as the angle of misorientation increases, the strain energy of the boundary decreases and the interfacial energy increases. Consequently the nucleation frequency of both  $\theta'$  and  $T_1$  decreases.

Returning to Park and Ardell's paper [6] they noted that for low angle grain boundaries:

- (i) the number density of  $\eta$  precipitates was high;
- (ii) the  $\eta$  precipitates were plate like;
- (iii) the number density of the  $\eta$  particles decreased as the angle of misorientation increased.

Hence, we propose that the major reason that  $\eta$  precipitates on grain boundaries is due to strain energy considerations, and that interfacial energy only plays a secondary role. This is consistent with the fact that, in common with  $\theta'$  and  $T_1$ , intragranular nucleation of the  $\eta$  phase occurs on dislocations (see e.g., [10]).

In contrast, we believe that the converse is true for the fcc/bcc systems examined by Luo and Weatherly [7], Monzen and Kitagawa [8], where the complex semicoherent nature of all interfacial orientations, e.g., see [11] would favor high angle grain boundary nucleation. Again, this is consistent with the findings of Monzen and Kitagawa [8] who showed that low angle boundaries were not efficient nucleation sites.

In summary, we believe that, for a second phase particle with a given habit plane, if strain energy in one dimension, perpendicular to the habit plane, is significant enough to hinder the nucleation process, then low angle boundaries will be better nucleation sites than high angle boundaries. Conversely, if strain can be essentially ignored, high angle boundary nucleation will be favored over low angle boundary nucleation.

## ACKNOWLEDGMENTS

The authors acknowledge the Office of Naval Research, Grant #N00014-91-J-1648 and the Alloy Technology Division of Alcoa Laboratories, Alcoa Center, PA for financial support.

## REFERENCES

- [1] Vaughan, D., Acta Met., 16, p. 563 (1967)

- [2] Simon, J. P. and Guyot P., J. Mat. Sci., 10, p. 1947 (1975)
- [3] Aaronson, H. I., Aaron, H. B and Kinsman, K. R., Metal., 4, p. 1 (1971)
- [4] Lee, J. K. and Aaronson, H. I., Acta Met., 23, p. 799 (1975)
- [5] Lee, J. K. and Aaronson, H. I., Acta Met., 23, p. 809 (1975)
- [6] Park, J. K. and Ardell, A. J. Acta Met., 37, p. 2399 (1986)
- [7] Luo, C. P. and Weatherly, G. C., Acta Met., 37, p. 791 (1989)
- [8] Monzen, R. and Kitagawa K., Scripta Met, 22, p. 173 (1988)
- [9] Parayil T. R., Ph.D. Thesis, The Pennsylvania State University, PA 16802, Pennsylvania, USA, (1986).
- [10] Lorimer, G. W., In: Precipitation Processes in Solids, (K. C. Russell and H. I. Aaronson, eds.), TMS-AME, Warrendale, USA, p. 87 (1978)
- [11] Luo, C. P. and Weatherly, G. E., Acta Met., 35 p. 1963 (1987).

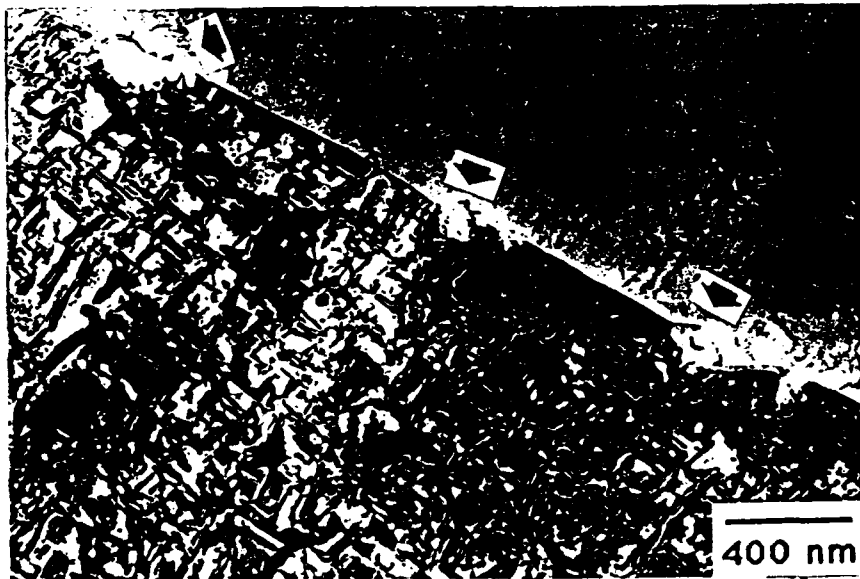


FIG 5. BF image of a typical high angle grain boundary. Only T<sub>2</sub> precipitates (arrowed) are found.

Microstructural Development of Sprayed Formed Aluminum/SiC  
During Aging

Xiaoli Tang and Paul R. Howell

Department of Materials Science and Engineering  
The Pennsylvania State University  
University Park, PA 16802

(Abstract)

The aluminum alloy 8090 has been used in many applications because of its high strength, excellent resistance to fatigue crack growth and good plane-stress fracture-toughness. With the addition of SiC, the strength can be increased and the density decreased. Hence an 8090 alloy matrix with SiC reinforcement has potential applications in aerospace engineering.

This paper will focus on the aging behavior of the 8090-SiC composite by comparing it with a controlled 8090 alloy. The materials have been aged for times up to 20 hours at 190°C. The mechanical property changes as a function of aging time have been monitored by microhardness-aging time curves (Figure 1). Some SEM investigations have been performed to document the distribution of SiC particles and the extent of grain boundary precipitation (Figure 2). Based on the different thermal expansion between the matrix and SiC, the matrix structure, e.g. dislocation density is affected by the addition of SiC. In addition, the interface structure between the matrix and SiC is important in determining the properties of the composite. Hence, conventional bright-field (BF) and centered dark-field (CDF) imaging together with weak-beam (WB) imaging will be presented to show the distribution of both dislocation loops and "punched-out" dislocations in the as-quenched condition. The same techniques will be used to examine how the interface changes during the aging process. This paper will give an evaluation concerning the dislocation distribution and the interfacial structure of this composite.

**SESSION: Interfaces/Interphases**

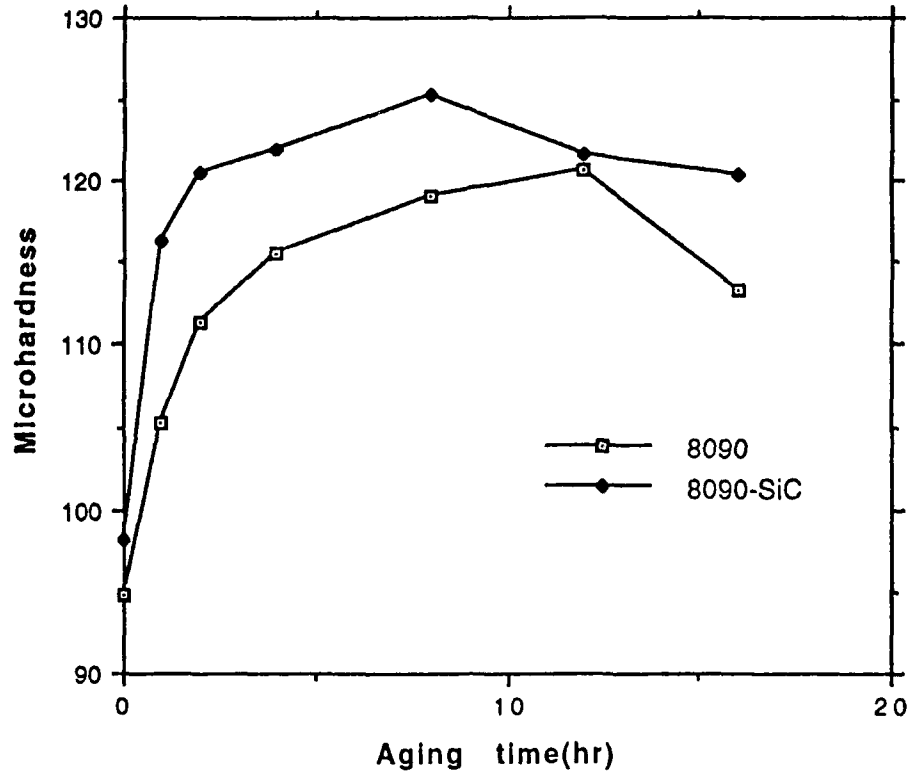


Figure 1 Aging Kinetic Curves

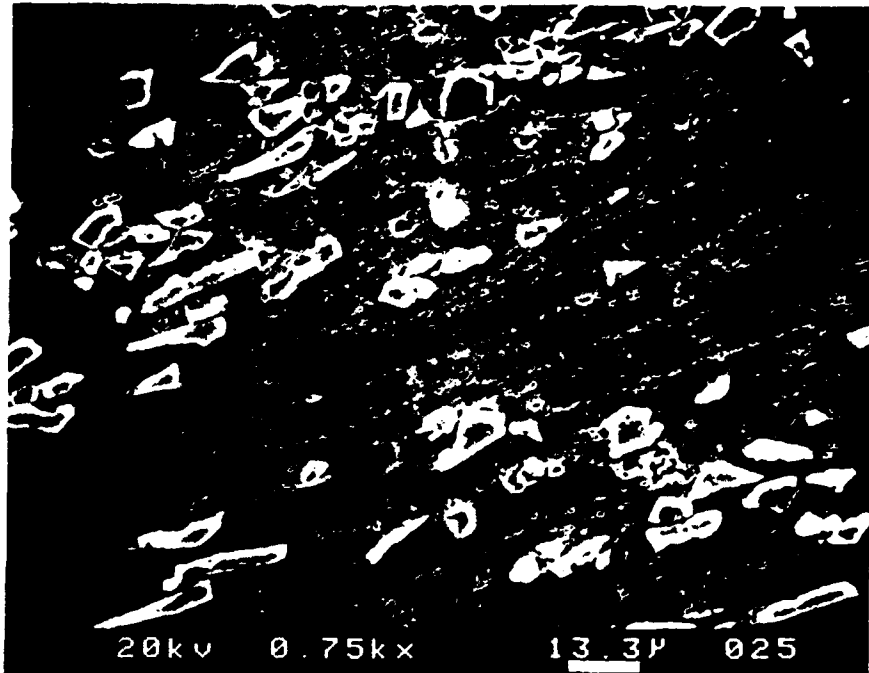


Figure 2 SEM Image of a Polished and Etched 8090-SiC Sample Aged 8 Hours at 190°C